Mass Spectrometric Methods for the Analysis of Nucleoside-Protein Cross-links: Application to Oxopropenyl-deoxyadenosine

Sarah C. Shuck, Kristie L. Rose, and Lawrence J. Marnett

Supporting Information

Contents:

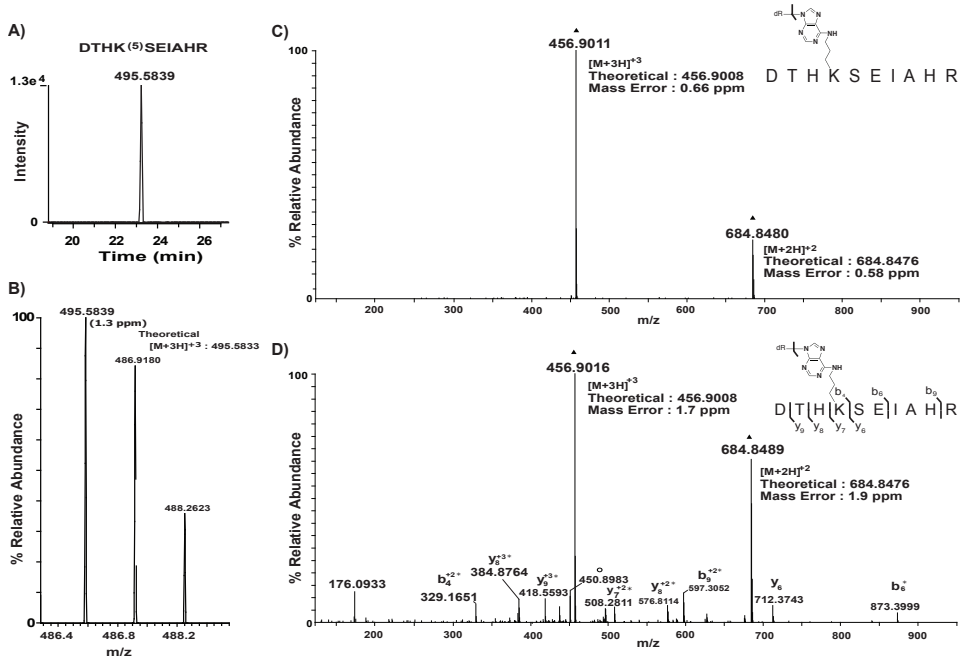

Supplemental Figure 1. Extracted ion chromatograms and corresponding MS spectra of precursor ions observed for OPdA-modified peptide DTHK$^{(5)}$SEIAHR. *A*, The XIC was generated as described in Figure 4A. *B*, The mass spectrum for the precursor peptide is annotated with the observed *m/z* values provided above the corresponding monoisotopic peak. The theoretical value of the precursor ion, adjacent to the observed peak, was used to calculate ppm mass error (shown in parentheses) for the identified peptide form. *C*, High-resolution targeted CID spectrum of precursor **5**-adducted DTHK$^{(5)}$SEIAHR peptide (m/z: 495.58). Dissociation of the glycosidic bond, as indicated by the bracket, results in the formation of intact peptide products with mass shifts consistent with **6**-adduction**.** This peptide is present as both doubly- and triply-protonated ions, denoted by▲. *D*, High-resolution targeted HCD spectrum of precursor **5**-adducted DTHK$^{(5)}$SEIAHR peptide (m/z: 495.58). Glycosidic bond cleavage was observed in addition to peptide backbone fragmentation. Asterisks indicate residues with mass shifts consistent with adduction by **6**. Water loss from the **6**-adducted DTHK$^{(6)}$SEIAHR product is denoted with ° , and the intact **6**-adducted DTHK$^{(6)}$SEIAHR peptide product is denoted with ▲. Mass errors observed for the $[M+2H]^{+2}$ and $[M+3H]^{+3}$ **6**-adducted peptide products are provided in both spectra and mass errors for all product ions observed were less than 4.5 ppm.

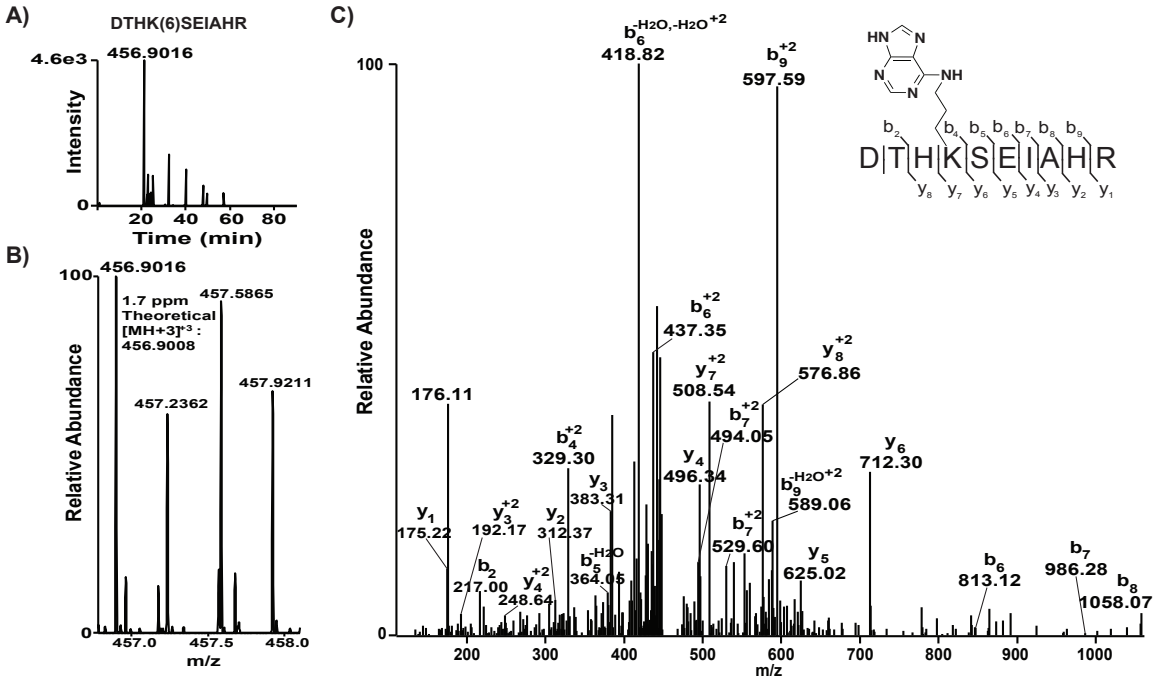

Supplemental Figure 2. Extracted ion chromatograms and corresponding MS and MS/MS spectra of precursor ions observed for OPdA-modified peptide DTHK$^{(6)}$SEIAHR. *A*, A window of ± 10 ppm around the theoretical *m/z* values for the observed precursor ion for peptide DTHK$^{(6)}$SEIAHR was used to generate the extracted ion chromatogram (XIC) shown. *B*, The mass spectrum for the precursor peptide is annotated with the observed *m/z* values provided above the corresponding monoisotopic peak. The theoretical value of the precursor ion, adjacent to the observed peak, was used to calculate ppm mass error (shown in parentheses) for the identified peptide form. *C*, CID spectrum of the **6**-adducted DTHK$^{(6)}$SEIAHR precursor peptide (m/z: 456.90). Brackets adjacent to the peptide sequence indicate sites of amide bond fragmentation at the peptide backbone that occurred with CID to generate b- and y-type product ions. Observed b- and y-ions are annotated above the corresponding product ion peaks in the spectrum. Asterisks indicate residues with mass shifts consistent with **6**-adduction.

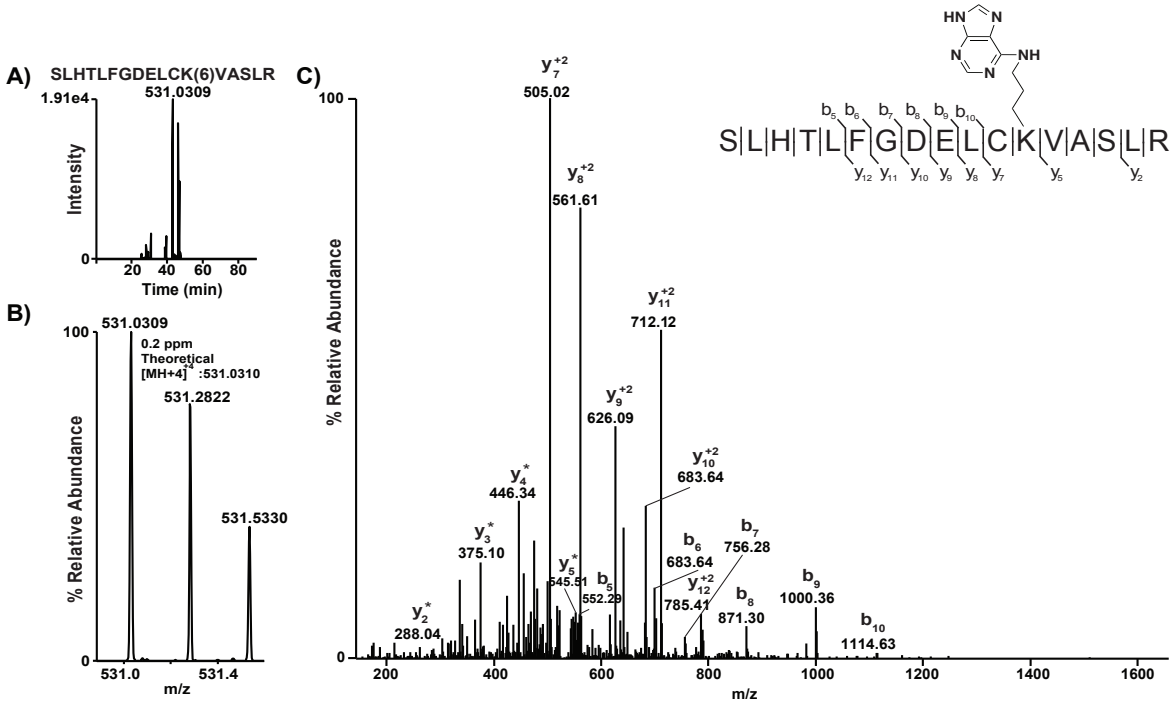

Supplemental Figure 3. Extracted ion chromatograms and corresponding MS and MS/MS spectra of precursor ions observed for OPdA-modified peptide SLHTLFGDELCK$^{(6)}$VASLR. *A*, A window of ± 10 ppm around the theoretical *m/z* values for the observed precursor ion for peptide SLHTLFGDELCK$^{(6)}$VASLR was used to generate the extracted ion chromatogram (XIC) shown. *B*, The mass spectrum for the precursor peptide is annotated with the observed *m/z* values provided above the corresponding monoisotopic peak. The theoretical value of the precursor ion, adjacent to the observed peak, was used to calculate ppm mass error (shown in parentheses) for the identified peptide form. *C*, CID spectrum of the **6**-adducted SLHTLFGDELCK$^{(6)}$VASLR precursor peptide (m/z: 531.03). Brackets adjacent to the peptide sequence indicate sites of amide bond fragmentation at the peptide backbone that occurred with CID to generate b- and y-type product ions. Observed b- and y-ions are annotated above the corresponding product ion peaks in the spectrum. Asterisks indicate residues with mass shifts consistent with **6**-adduction.

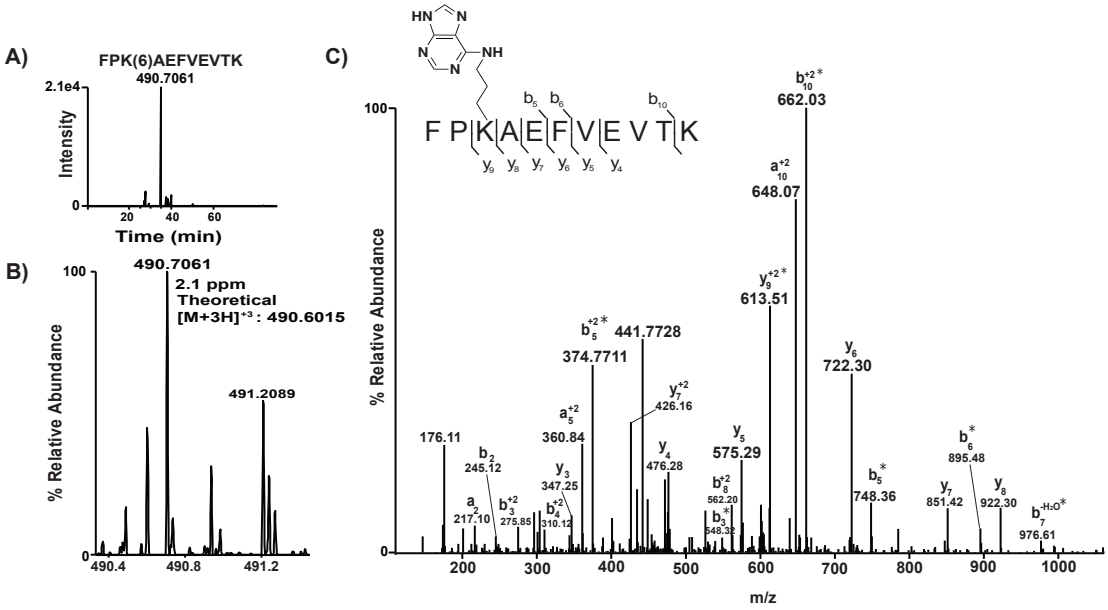

Supplemental Figure 4. Extracted ion chromatograms and corresponding MS and MS/MS spectra of precursor ions observed for OPdA-modified peptide FPK$^{(6)}$AEFVEVTK. *A*, A window of ± 10 ppm around the theoretical *m/z* values for the observed precursor ion for peptide FPK$^{(6)}$AEFVEVTK was used to generate the extracted ion chromatogram (XIC) shown. *B*, The mass spectrum for the precursor peptide is annotated with the observed *m/z* values provided above the corresponding monoisotopic peak. The theoretical value of the precursor ion, adjacent to the observed peak, was used to calculate ppm mass error (shown in parentheses) for the identified peptide form. *C*, CID spectrum of the **6**-adducted FPK$^{(6)}$AEFVEVTK precursor peptide (m/z: 490.71). Brackets adjacent to the peptide sequence indicate sites of amide bond fragmentation at the peptide backbone that occurred with CID to generate b- and y-type product ions. Observed b- and y-ions are annotated above the corresponding product ion peaks in the spectrum. Asterisks indicate residues with mass shifts consistent with **6**-adduction.

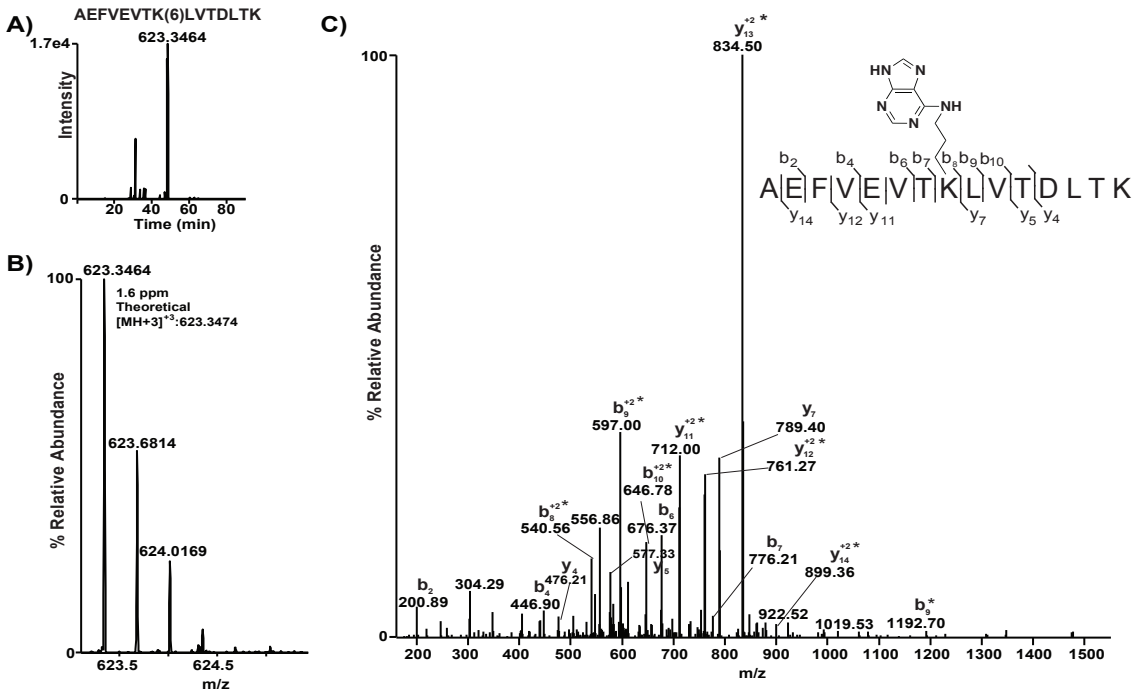

Supplemental Figure 5. Extracted ion chromatograms and corresponding MS and MS/MS spectra of precursor ions observed for OPdA-modified peptide AEFVEVTK$^{(6)}$LVTDLTK. *A*, A window of ± 10 ppm around the theoretical *m/z* values for the observed precursor ion for peptide AEFVEVTK$^{(6)}$LVTDLTK was used to generate the extracted ion chromatogram (XIC) shown. *B*, The mass spectrum for the precursor peptide is annotated with the observed *m/z* values provided above the corresponding monoisotopic peak. The theoretical value of the precursor ion, adjacent to the observed peak, was used to calculate ppm mass error (shown in parentheses) for the identified peptide form. *C*, CID spectrum of the **6**-adducted AEFVEVTK$^{(6)}$LVTDLTK precursor peptide (m/z: 623.35). Brackets adjacent to the peptide sequence indicate sites of amide bond fragmentation at the peptide backbone that occurred with CID to generate b- and y-type product ions. Observed b- and y-ions are annotated above the corresponding product ion peaks in the spectrum. Asterisks indicate residues with mass shifts consistent with **6**-adduction.

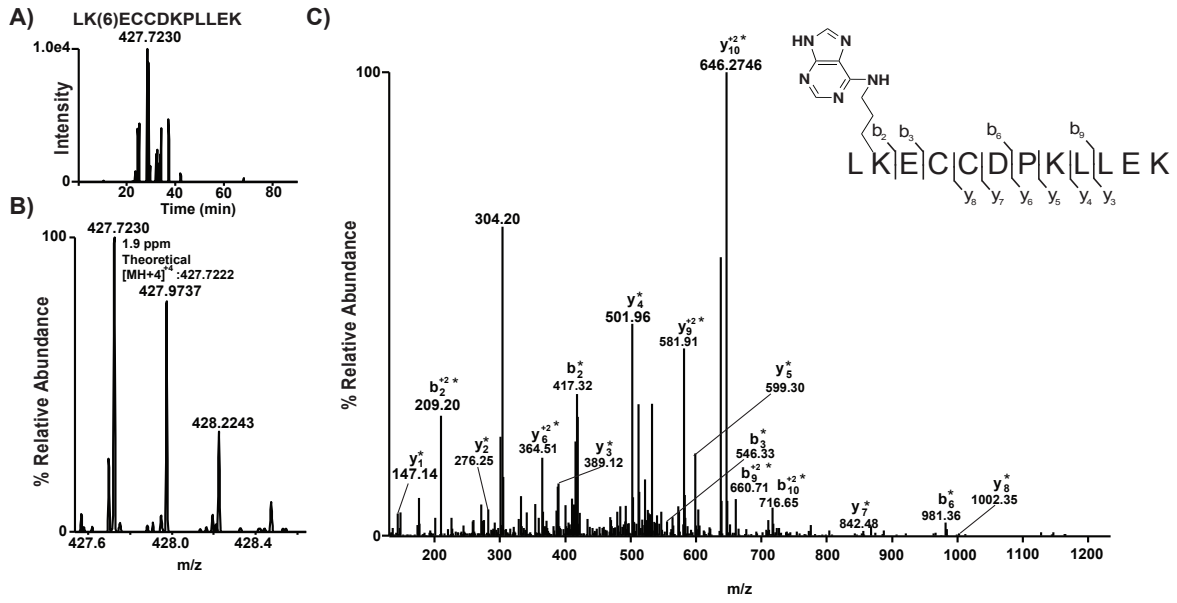

Supplemental Figure 6. Extracted ion chromatograms and corresponding MS and MS/MS spectra of precursor ions observed for OPdA-modified peptide LK$^{(6)}$ECCDPKLLEK. *A*, A window of ± 10 ppm around the theoretical *m/z* values for the observed precursor ion for peptide LK$^{(6)}$ECCDPKLLEK was used to generate the extracted ion chromatogram (XIC) shown. *B*, The mass spectrum for the precursor peptide is annotated with the observed *m/z* values provided above the corresponding monoisotopic peak. The theoretical value of the precursor ion, adjacent to the observed peak, was used to calculate ppm mass error (shown in parentheses) for the identified peptide form. *C*, CID spectrum of the **6**-adducted LK$^{(6)}$ECCDPKLLEK precursor peptide (m/z: 427.72). Brackets adjacent to the peptide sequence indicate sites of amide bond fragmentation at the peptide backbone that occurred with CID to generate b- and y-type product ions. Observed b- and y-ions are annotated above the corresponding product ion peaks in the spectrum. Asterisks indicate residues with mass shifts consistent with **6**-adduction.

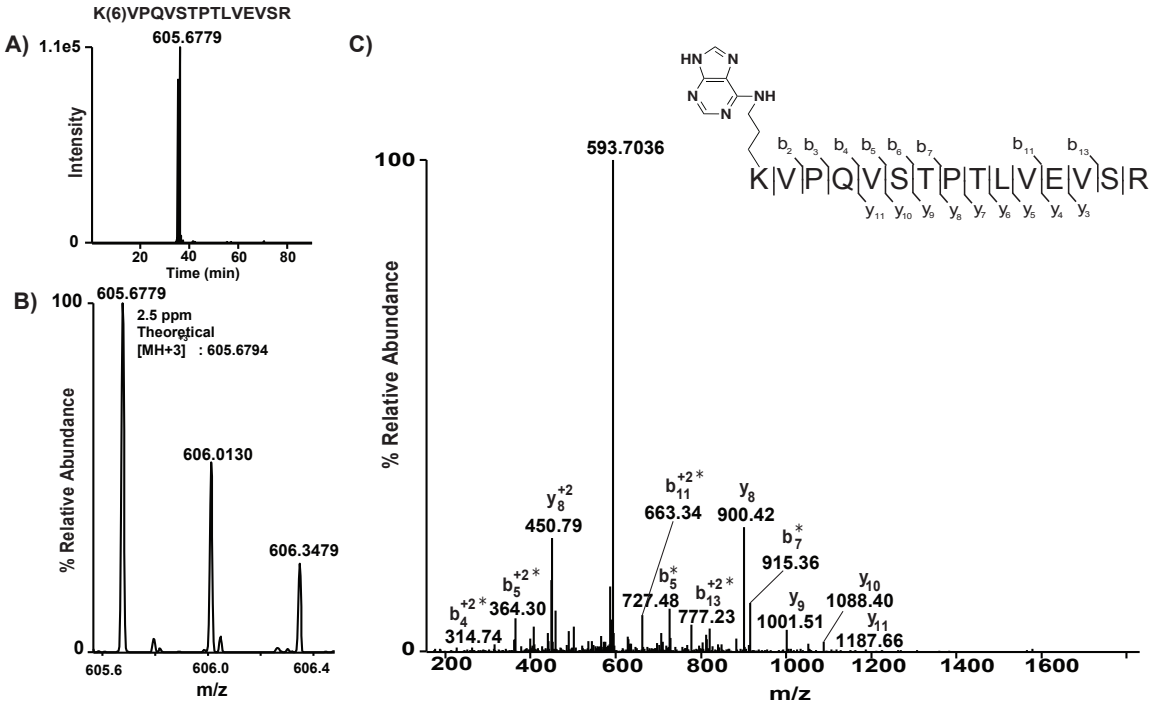

Supplemental Figure 7. Extracted ion chromatograms and corresponding MS and MS/MS spectra of precursor ions observed for OPdA-modified peptide K$^{(6)}$VPQVSTPTLVEVSR. *A*, A window of ± 10 ppm around the theoretical *m/z* values for the observed precursor ion for peptide K$^{(6)}$VPQVSTPTLVEVSR was used to generate the extracted ion chromatogram (XIC) shown. *B*, The mass spectrum for the precursor peptide is annotated with the observed *m/z* values provided above the corresponding monoisotopic peak. The theoretical value of the precursor ion, adjacent to the observed peak, was used to calculate ppm mass error (shown in parentheses) for the identified peptide form. *C*, CID spectrum of the **6**-adducted K$^{(6)}$VPQVSTPTLVEVSR precursor peptide (m/z: 605.68). Brackets adjacent to the peptide sequence indicate sites of amide bond fragmentation at the peptide backbone that occurred with CID to generate b- and y-type product ions. Observed b- and y-ions are annotated above the corresponding product ion peaks in the spectrum. Asterisks indicate residues with mass shifts consistent with **6**-adduction.

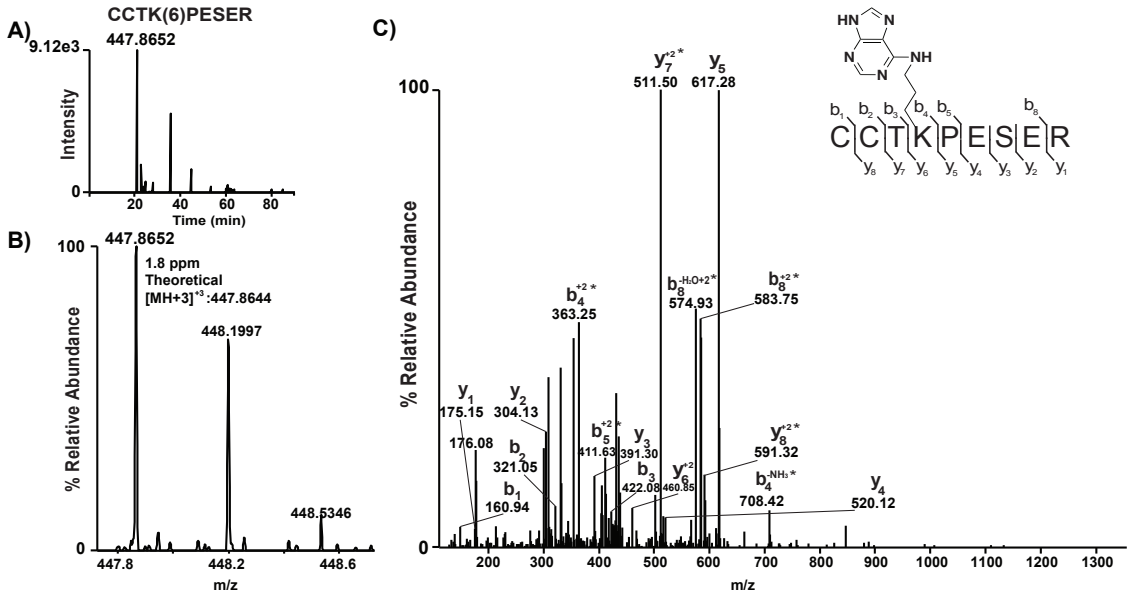

Supplemental Figure 8. Extracted ion chromatograms and corresponding MS and MS/MS spectra of precursor ions observed for OPdA-modified peptide CCTK$^{(6)}$PESER *A*, A window of ± 10 ppm around the theoretical *m/z* values for the observed precursor ion for peptide CCTK$^{(6)}$PESER was used to generate the extracted ion chromatogram (XIC) shown. *B*, The mass spectrum for the precursor peptide is annotated with the observed *m/z* values provided above the corresponding monoisotopic peak. The theoretical value of the precursor ion, adjacent to the observed peak, was used to calculate ppm mass error (shown in parentheses) for the identified peptide form. *C*, CID spectrum of the **6**-adducted CCTK$^{(6)}$PESER precursor peptide (m/z: 447.86). Brackets adjacent to the peptide sequence indicate sites of amide bond fragmentation at the peptide backbone that occurred with CID to generate b- and y-type product ions. Observed b- and y-ions are annotated above the corresponding product ion peaks in the spectrum. Asterisks indicate residues with mass shifts consistent with **6**-adduction.

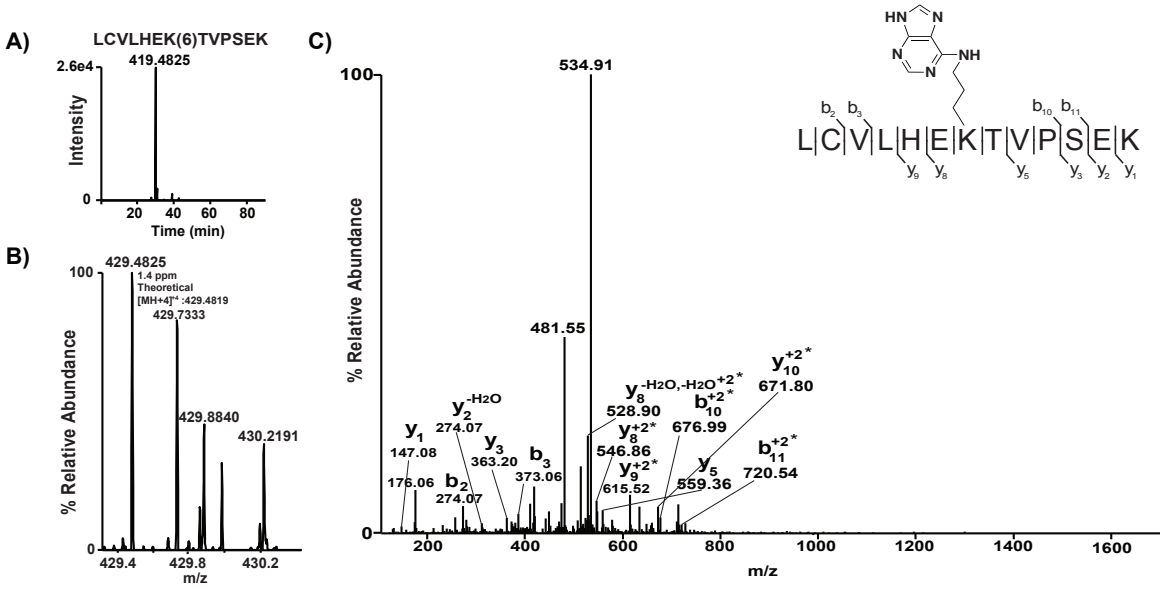

Supplemental Figure 9. Extracted ion chromatograms and corresponding MS and MS/MS spectra of precursor ions observed for OPdA-modified peptide LCVLHEK$^{(6)}$TVPSEK *A*, A window of ± 10 ppm around the theoretical *m/z* values for the observed precursor ion for peptide LCVLHEK$^{(6)}$TVPSEK was used to generate the extracted ion chromatogram (XIC) shown. *B*, The mass spectrum for the precursor peptide is annotated with the observed *m/z* values provided above the corresponding monoisotopic peak. The theoretical value of the precursor ion, adjacent to the observed peak, was used to calculate ppm mass error (shown in parentheses) for the identified peptide form. *C*, CID spectrum of the **6**-adducted LCVLHEK$^{(6)}$TVPSEK precursor peptide (m/z: 429.48). Brackets adjacent to the peptide sequence indicate sites of amide bond fragmentation at the peptide backbone that occurred with CID to generate b- and y-type product ions. Observed b- and y-ions are annotated above the corresponding product ion peaks in the spectrum. Asterisks indicate residues with mass shifts consistent with **6**-adduction.

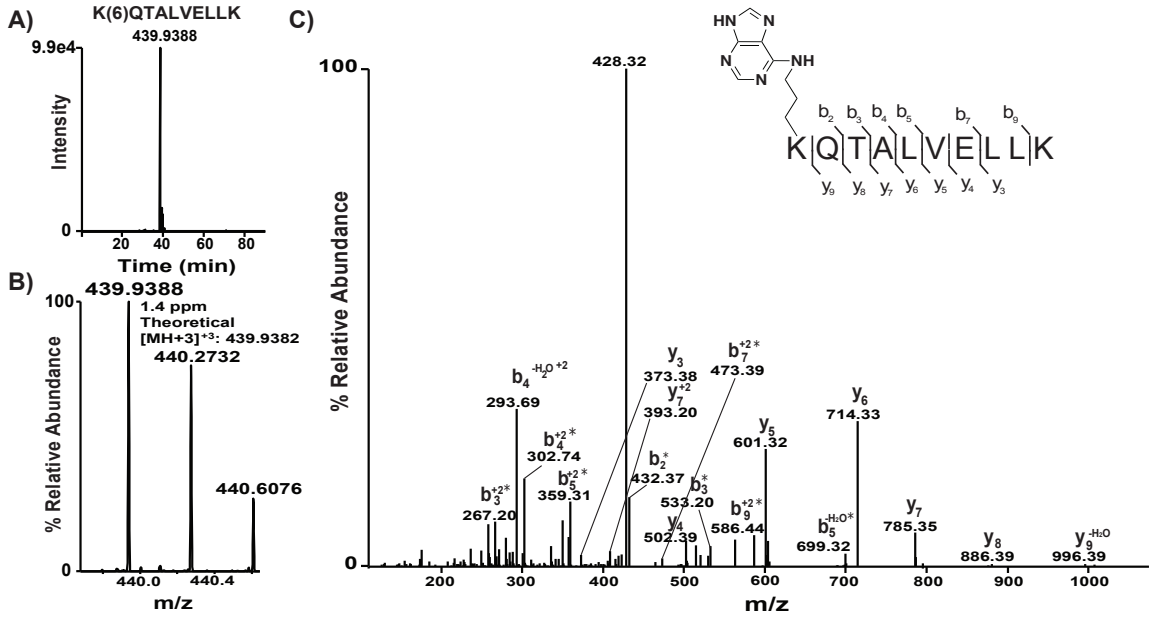

Supplemental Figure 10. Extracted ion chromatograms and corresponding MS and MS/MS spectra of precursor ions observed for OPdA-modified peptide K$^{(6)}$QTALVELLK *A*, A window of ± 10 ppm around the theoretical *m/z* values for the observed precursor ion for peptide K$^{(6)}$QTALVELLK was used to generate the extracted ion chromatogram (XIC) shown. *B*, The mass spectrum for the precursor peptide is annotated with the observed *m/z* values provided above the corresponding monoisotopic peak. The theoretical value of the precursor ion, adjacent to the observed peak, was used to calculate ppm mass error (shown in parentheses) for the identified peptide form. *C*, CID spectrum of the **6**-adducted K$^{(6)}$QTALVELLK precursor peptide (m/z: 439.94). Brackets adjacent to the peptide sequence indicate sites of amide bond fragmentation at the peptide backbone that occurred with CID to generate b- and y-type product ions. Observed b- and y-ions are annotated above the corresponding product ion peaks in the spectrum. Asterisks indicate residues with mass shifts consistent with **6**-adduction.

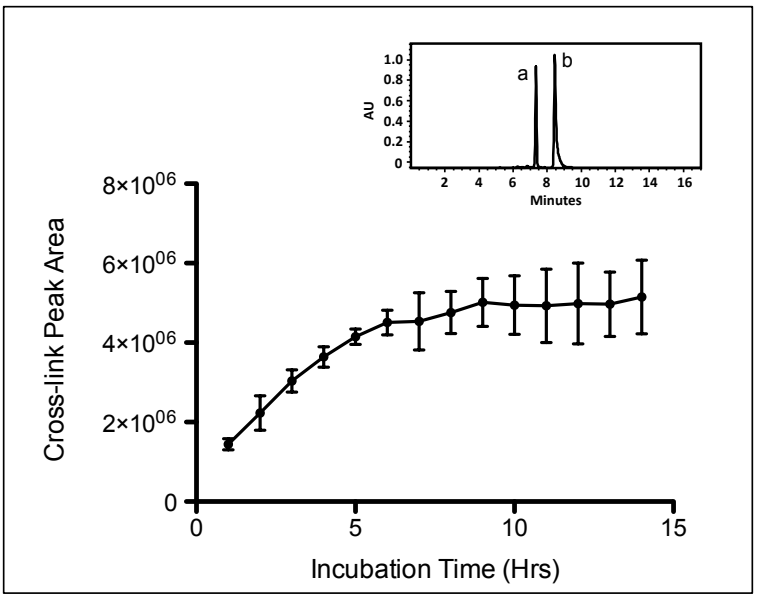

Supplemental Figure 11. HPLC analysis of OPdA and *N*-α-acetyllysine cross-link formation. OPdA and N-α-acetyllysine were incubated for the indicated time points, and cross-link formation was monitored using photodiode array HPLC as described in Experimental Procedures. The peak area was determined using Empower software and data were obtained from 3 independent experiments. The inset displays the HPLC chromatogram obtained at the 6-hr time point with peaks corresponding to OPdA at 8.5 min (b) and the OPdA-*N*-α-acetyllysine cross-link at 7.4 min (a).